Journal of Alloys and Compounds 515 (2012) 101–107

Contents lists available at SciVerse ScienceDirect

Journal of Alloys and Compounds

journal homepage: www.elsevier.com/locate/jallcom

Optical and photoconductive properties of $Pb_{0.9}Sn_{0.1}Se$ nano-structured thin films deposited by thermal vacuum evaporation and pulsed laser deposition

Sara Gad [a], M. Abdel Rafea [a,*], Yehia Badr [b]

[a] Electronic Materials Department, Advanced Technology & New Materials Institute, City for Scientific Research and Technology Applications, P.O. Box 21934, New Borg El-Arab, Alexandria, Egypt
[b] National Institute of Laser Enhanced Science, Laser Interaction with Matter Department, Cairo University, Cairo, Egypt

ARTICLE INFO

Article history:
Received 20 September 2011
Received in revised form
17 November 2011
Accepted 22 November 2011
Available online 30 November 2011

Keywords:
$Pb_{0.9}Sn_{0.1}Se$ thin films
Thermal evaporation
Pulsed laser deposition
Optical properties
Photoconductivity

ABSTRACT

In this work, thin films of $Pb_{0.9}Sn_{0.1}Se$ were deposited by thermal vacuum evaporation and pulsed laser deposition techniques. XRD measurements reveal a cubic crystalline structure for the prepared powder and deposited films. SEM micrographs show that the films consist of fine grains of size in the nanoscale. EDX analysis confirms the compositional analysis of both powder and films. Both the optical and photoconductive properties of those films were studied for comparison. Free carrier absorption was observed in the thermally evaporated films which were reduced by vacuum annealing at 773 K for 1 h under as a result of removing defects. The optical band gap of the thermally evaporated films was also reduced by annealing which was explained by removal of a Burstein–Moss shift. A strong increase of band gap of films deposited by pulsed laser technique was also aberved while it was explained by enegy gap confinment effect associated with nanostructures of semiconducting materials. Photoconductivity measurment shows that the photosensitivity of the pulsed laser deposited films is higher than those of the thermally deposited films by five order of magnitude. While the photoconduction process of thermally evaporated films is slower than that in pulsed laser deposited films.

1. Introduction

The IV–VI compound systems based on lead, Sn and Se are important class of narrow band gap semiconductors that have potentials applications in optoelectronics device [1–8]. Such applications are IR laser diodes and photo detectors working in the wavelength range 3–30 μm. This IR spectral range can be covered either by change the Pb–Sn composition from 0.0 to 0.45 that the absorption edge of the compound decreases as composition increases or by partially replacement of the selenium atom by tellurium [9–11]. $Pb_{1-x}Sn_xSe$ system is a cubic crystal structure with direct band gap. Many techniques were used in order to deposit IV–VI chalcogenides for different applications such as IR thermal imaging [12–14]. The quite nearest reported material for $Pb_{0.9}Sn_{0.1}Se$ is the PbSe. PbSe monocrytalline layer deposited by molecular beam epitaxial growth possesses carriers lifetime in the range 10–20 μs near the room temperature [15].

This carriers lifetime is obtained using the photoconductivity measurements of the rise and decay relaxation peaks. This value is close to the single crystalline material which possesses single carrier type and single scattering mechanism. The carriers lifetime depends upon many parameters such as temperature and type of scattering process. Polycrystalline and/or nanocrystalline materials possess different scattering processes. Carriers scattering process is predominated by grain boundaries which reduces the carrier's mobility from several thousands to few $cm^2/V\,s$ consequently the corresponding mean free path of carriers generation and recombination is then changed which reduces the apparent carriers lifetime to longer value than in single crystalline material. Long-term carriers lifetime can be observed in photoconduction experiment at lower light chopping. At higher frequencies of light chopping the intrinsic or other carrier lifetime process can be also observed. Deposition technique of chalcogenide materials was found recently controlling the deposited film properties. Many reports in lead selenide and its ternary compounds were deposited by chemical solution growth techniques [16–21], molecular beam epitaxy, MBE [22–25], electrochemical deposition [26], sol–gel technique [27], thermal evaporation [28,29], thermal reduction method [30], hydrothermal synthesis [31] and colloidal solution [32]. Each technique treats a specific problem such nano architecting, nano devices, wide area, ease preparation, nano particles and colloide, respectively. Reports of composition control by flash evaporation, thermal vacuum deposition and electron beam evaporation techniques have been also performed [33–35]. Thermal evaporation was observed to produces good quality film although flash evaporation technique was observed to control the

* Corresponding author. Tel.: +20 3 4593414; fax: +20 3 4593414.
E-mail address: m.abdelrafea@mucsat.sci.eg (M.A. Rafea).

0925-8388/$ – see front matter © 2011 Elsevier B.V. All rights reserved.
doi:10.1016/j.jallcom.2011.11.100

composition better while the film structures is multi-layers. Electron beam deposition technique collects the two advantages that control the composition and produces single continuous layer. The aim of this work is to deposit $Pb_{0.9}Sn_{0.1}Se$ thin films under vacuum by two different deposition techniques such as pulsed laser and thermal evaporation. The comparison between those films is taken into account by studying the structural, optical, electrical and photoconductive properties of those films.

2. Experimental procedure

Pure elements of Pb, Sn, and Se of 5 N (Alfa Aesar GmbH & Co) were used in the preparation of $Pb_{0.9}Sn_{0.1}Se$ ingot material. Appropriate weights of Pb, Sn, and Se were chosen to produce composition at $x = 0.1$ then they are mixed and poured in a clean silica ampoule closed from one side. The ampoule was evacuated from the other side at 10^{-4} Torr and sealed by wilding a narrow nick which was made before. The ampoule was heated in a muffle under two temperature programs that were suggested for safe and homogenous preparation of the material. The first program has a final temperature around the melting point of selenium which is characterized by a smaller rate and longer time spent at higher temperature. The second program starts normally after cooling down without afraid of selenium vapor pressure increment because Se is then partially reacted with Sn, Pb or both of them. In the second heating program, the temperature was increased until 1373 K and fixed 3 h at this temperature. During the temperature rising and reaction process, the ampoule was shacked up and down and rotated vertically every 15 min in order to homogenize the reactants. The molten material was cooled down below the melting point at 1355 K with high cooling rate by ambient in order to prevent segregation. After cooling down to room temperature, the ampoule was broken and the ingot material was collected in an agate mortar then crushed to fine powder. Two tablets were prepared by hydrostatic press at 8 ton/cm^2 under vacuum in order to be used as the material source. The first tablet was evaporated in a Mo boat under high vacuum of 10^{-6} Torr using a standard Edwards A306 Auto coater with conventional rotary and turbo molecular pumps. The evaporation process was optimized at evaporation rate 10 Å/s and the heating current pass through the boat was 2.8–3.0 A. The second tablet was evaporated by Pulsed laser deposition system. A XeCl pulsed laser beam of wavelength 308 nm and energy 4 J entered a quartz window. About 50,000 pulses were used in evaporation of the rotated tablet of the ingot material. The substrates were supported on rotating disc holder during evaporation process in both two techniques. The substrates were selected to be glass slides, single crystals of KBr crystals and pressed polycrystalline powder of KBr. A standard cleaning procedure was applied on both the glass slides and the silica tubes of the ingot material preparation. Both the glass substrates and ampoules were cleaned several times using ultrasonic cleaner, detergent, double distilled water and final washing with ethanol, respectively. XRD measurements were performed using X-ray diffractometer of type Shimadzu 7000 maxima powder diffraction under the measurement conditions of X-ray tube voltage was 30 kV, current was 30 mA, wavelength Cu Kα1 λ = 1.5406 Å and the scan range was 5–90° with scan speed 1°/min. SEM of type "Jeol-JSM-636 OLA" was used for studying the surface morphology of the deposited films. The cross sectional image of the film-substrate interface was studied in order to examine the film adhesion and determine the film thickness at different points of the broken edge. Besides, EDX (Energy dispersive X-ray spectroscopy) technique used for the composition of the powder and films. FT-IR of type Shimadzu 8400 was used for studying the optical transmittance of the films and reference substrate was also used. Photoconductivity experiment was constructed using a set of mirrors that reflect and focus the light source. Tungsten-halogen lamp of power 20 W working at 12 V was used as wide spectral range light source. The filament emits the visible region to near infrared region of the spectrum while the heated quartz envelop of the bulb re-emit the far IR range.

3. Results and discussions

3.1. Structure

X-ray diffraction patterns presented in Fig. 1 show that the ingot materials and all deposited films are polycrystalline structure. The calculated interplanar spacing, d (Å) were compared with those in the standard card of PbSe–SnSe solid solution cubic systems, Card No. [00-071-6518 for $x = 0.2$, 01-071-6517 for $x = 0.4$, 00-002-0588 for $x = 0$, 00-001-0848 for Se, 00-014-0159 for SnSe of the ICDDVIEW 2006 data base]. The calculated compositions in between shows that those d-values and corresponding unit cell dimension, a (Å) which agree well with the $Pb_{1-x}Sn_xSe$ at composition, $x = 0.11$. The corresponding hkl of the PbSnSe solid solution were then identified as shown in Fig. 1. It was observed that a trace of SnSe diffracted peak was probably found in the

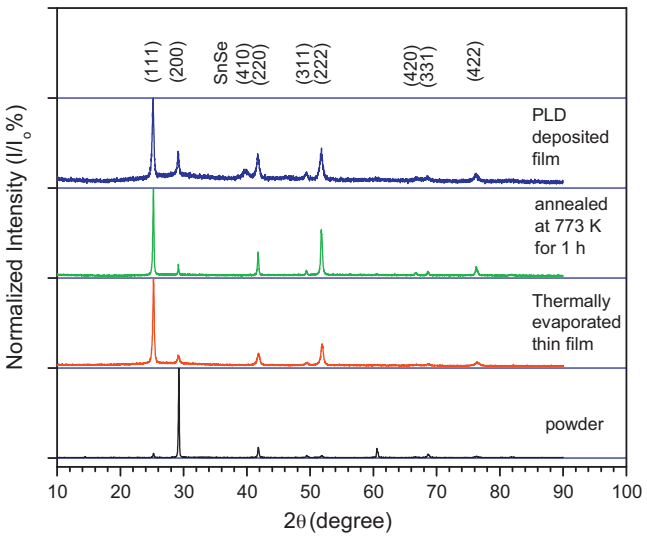

Fig. 1. XRD patterns of $Pb_{0.9}Sn_{0.1}Se$ powder and thin films.

pulsed laser deposited film which belongs to the (4 1 1) orientation, while the other diffracted peaks for powder and films belong to the PbSnSe phase at composition $x = 0.1$. Powder material possesses a preferred orientation at (2 0 0) in which the crystallites grown along this direction. The thin films deposited by pulsed laser and thermal evaporation techniques were grown along the (1 1 1) direction. Annealing of the films at 773 K for 1 h increases the preferentiality while other peak intensities decrease except the parallel planes (1 1 1) and (2 2 2). Pulsed laser deposited film diffraction pattern is characterized by observable background due to lower crystallinity and broadening in the diffracted peaks. Peak broadening was studied in the rule of microstrain-crystallite size relationship. The Williamson–Hall equation [36] was used in order to determine the crystallite size as follows:

$$\beta \cos\theta = 4\eta \sin\theta + \frac{K\lambda}{D} \quad (1)$$

where β is the broadening of the diffracted peak and equal to $\sqrt{\beta^2_{\text{sample}} - \beta^2_{\text{silicon}}}$. β_{sample} is the measured broadening for sample and β_{silicon} is the measured broadening for silicon single crystal free from defects in order to eliminate the instrumental broadening. Broadening was measured at peak width at half maximum intensity of the diffracted peak. η is the microstrain, K is a shape factor close to unity, λ is the X-ray wavelength and D is the crystallite size. Eq. (1) has two unknown parameters, they are the crystallite size and microstrain. Plotting $\beta\cos\theta$ vs. $\sin\theta$ produces a straight line of slope is 4η and intercept is $K\lambda/D$ in which the crystallite size can be determined as represented in Fig. 2. Powder was found to be negligible microstrain with average crystallite size about 95 nm. Thin films deposited by thermal evaporation possess crystallite size of 68 nm and lattice strain of 2.4×10^{-3}. Annealing this film increases the crystallite size to be 72 nm due to crystallite growth, besides the effect was clearly noticed in reducing the microstrain to be 4.6×10^{-4} due to crystallites relaxation by annealing. The crystallite size of the pulsed laser deposited film was found to be 40 nm. This small value of crystallite size may come from preventing the growth process during pulsed vaporization and condensation of the evaporated material caused by the pulsed laser beam. In the other side, the lattice strain in this film was found to be 5.9×10^{-4}. According to X-ray measurements, it can be concluded that the deposition by thermal evaporation technique of PbSnSe produces low strain if annealed, while the obtained crystallites is bigger. At both low

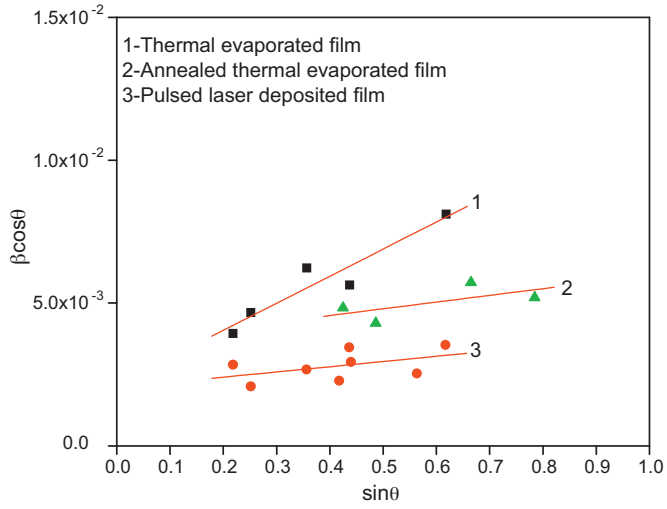

Fig. 2. Williamson–Hall rule for lattice strain and crystallite size determination for $Pb_{0.9}Sn_{0.1}Se$ films.

strain films, the average crystallite size of thermal evaporated and pulsed laser deposited films were 72 nm, respectively.

3.2. Compositional analysis and surface morphology

The calculated elemental ratio using standard less analysis (ZAF) and the atomic percentages were measured by EDX technique. The comparison between the theoretical calculated composition from the materials weighing before preparation and the measured composition by the EDX is represented in Table 1. It was noticed that excess Se was observed in both powder and thin films at the surface. This indicates that Se may be accumulated near the surface while their amount does not exceed 4–5%. The other observation is that there is high similarity between powder, thermal vacuum deposited films and pulsed laser deposition films in their chemical composition. This indicates that the composition is well controlled

Table 1
EDX analysis of $Pb_{0.9}Sn_{0.1}Se$ material.

Sample	$X_{Theoretical}$	Pb%	Sn%	Se%	$X_{Experimental}$
Powder	0.1	42.34	5.48	52.18	0.124
Film deposited by thermal evaporation	0.1	41.57	5.67	52.76	0.120
Film deposited by PLD	0.1	41.08	5.33	53.59	0.115

by the used preparation techniques. Three different magnified images of the films surfaces were performed, besides cross sectional imaging of the films at broken edge for film thickness measurement and film adhesion to the substrate. These images are presented for thermally evaporated films and pulsed laser deposited films as shown in Figs. 3 and 4, respectively. It was observed that the film surface structure consists of fine and compact grains of size in the range 50–70 nm. Besides, there were no cracks or peels observed at the film surfaces. The cross sectional images of the film show the two parallel surfaces structure. The thicknesses of the films were 290 nm and 115 nm for thermally evaporated and pulsed laser deposited films, respectively. Also there was a good adhesion and high film coverage on the substrate.

3.3. Optical properties

The optical transmittances of the $Pb_{0.9}Sn_{0.1}Se$ films were measured in the FT-IR spectrophotometer are represented in Fig. 5. These films were deposited on IR transparent substrate made from KBr pressed powder and BaF_2 crystals cleaved at (1 1 1) plane. It was observed that film deposited by thermal vacuum evaporation technique and the annealed film contains interference fringes, while the pulsed deposited film did not contain. The contribution of film thickness on the interference fringes is then clear. It was difficult to increase the film thickness in the pulsed laser deposition process unless depositing for longer time, besides deposition for shorter time in the thermal evaporation technique is not preferable due to perturbation in evaporation rate. When the thermal evaporated film annealed at 773 K for 1 h, the absorption edge are shifted towards the longer wavelengths. A small absorption process occurs

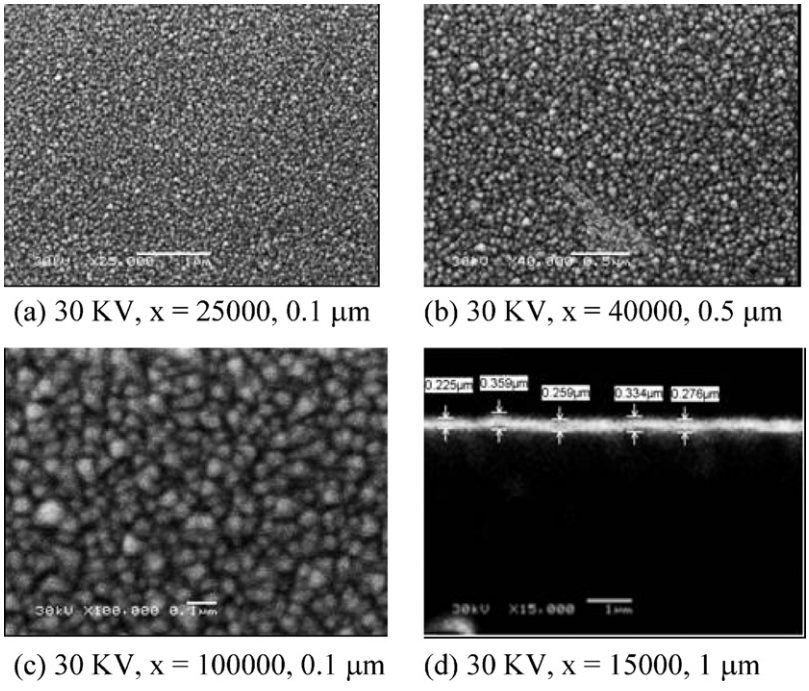

Fig. 3. SEM of $Pb_{0.9}Sn_{0.1}Se$ thin film deposited on glass substrate.

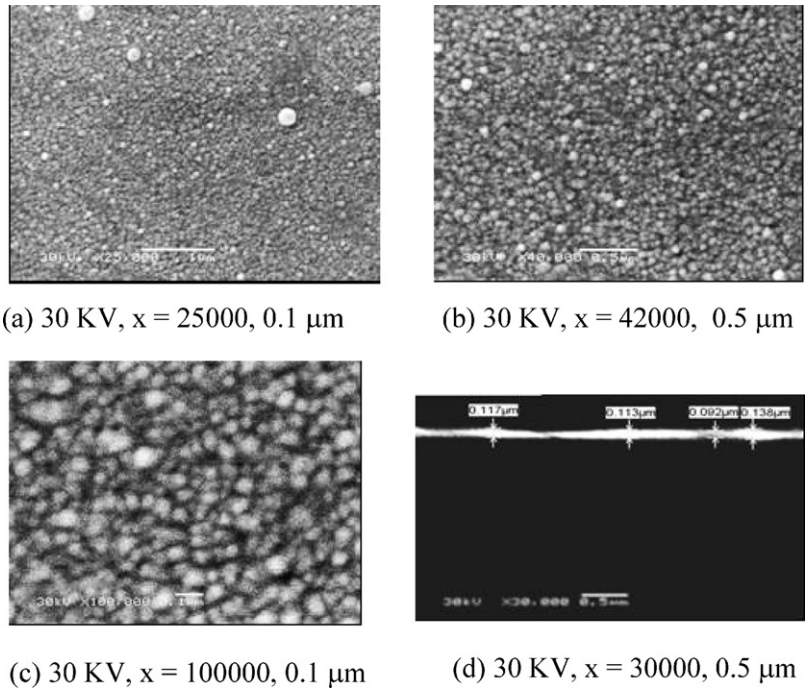

Fig. 4. SEM of $Pb_{0.9}Sn_{0.1}Se$ thin film deposited on glass by PLD.

below the band edge (at long wavelength) in the un-annealed film which was observed from the transmittance curve while annealing process eliminates it. Generally, absorption process at longer wavelength below the band gap is a contribution of the free carrier absorption as results of high carriers concentration. The transmittance of the pulsed laser deposited film was observed to be high in both absorption and dispersion region. The absorption coefficient α is calculated from the optical transmittance directly using the film thickness measured by the cross sectional image of the SEM. The optical band gap, E_g, is a critical parameter that governs the absorption process given as follows:

$$\alpha = B\frac{\sqrt{h\nu - E_g}}{h\nu} \quad (2)$$

where B is constant, $h\nu$ is the incident photon energy. The band gap was determined by plotting $(\alpha h\nu)^2$ vs. $h\nu$ in the direct transition of PbSnSe system. A straight line is produced near the absorption edge region whose intercept on the abscissa at the band gap. Fig. 6 represents the plots of $(\alpha h\nu)^2$ vs. $h\nu$ for films deposited by thermal vacuum evaporation and pulsed laser deposition techniques, respectively. The band gaps were found to be 0.14 and 0.26 eV for thermally evaporated film and pulsed deposited film, respectively. While annealing of the thermally deposited film at 773 K for 1 h reduces the band gap to be 0.12 eV as shown in Fig. 7. The $Pb_{0.9}Sn_{0.1}Se$ band gap is in the range 0.11–0.12 depending on composition fluctuation due to high sensitivity of the absorption edge to the composition. Band gap of the annealed film of 0.12 eV is considered as the nearest value of the $Pb_{0.9}Sn_{0.1}Se$ band gap. The calculated band gap of the pulsed laser deposited film is much higher than in thermally deposited film. Besides, both of them are deviated from the band gap of $Pb_{0.9}Sn_{0.1}Se$ semiconducting

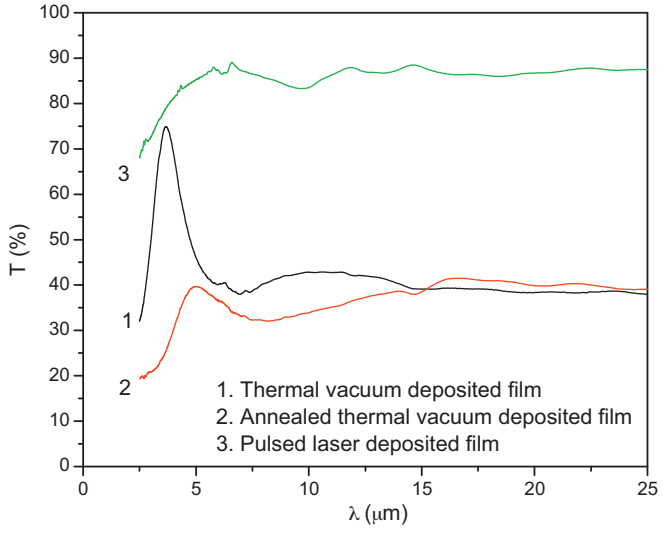

Fig. 5. IR optical transmittance of $Pb_{0.9}Sn_{0.1}Se$ films deposited on KBr pressed powder.

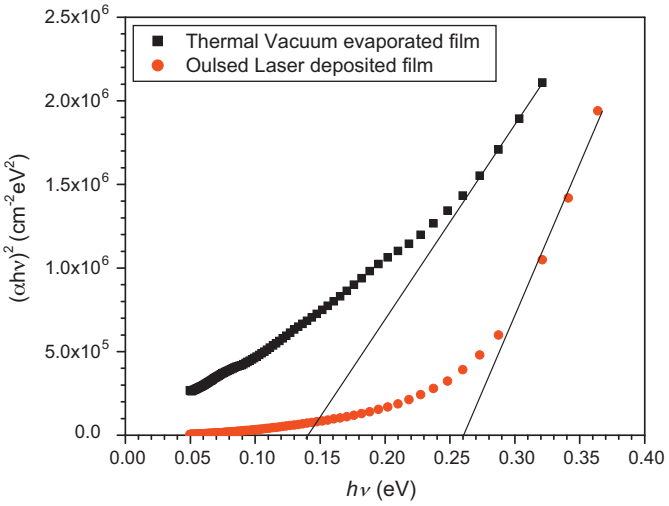

Fig. 6. $(\alpha h\nu)^2$ vs. $h\nu$ of $Pb_{0.9}Sn_{0.1}Se$ film as deposited films.

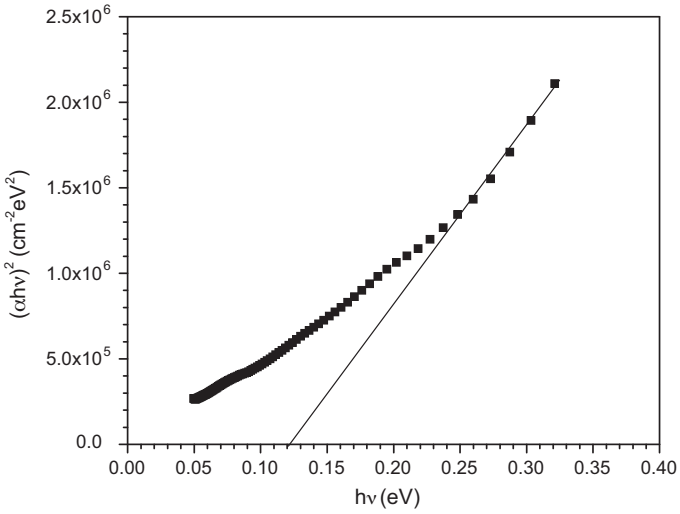

Fig. 7. $(\alpha h\nu)^2$ vs. $h\nu$ of $Pb_{0.9}Sn_{0.1}Se$ annealed film deposited by thermal evaporation technique.

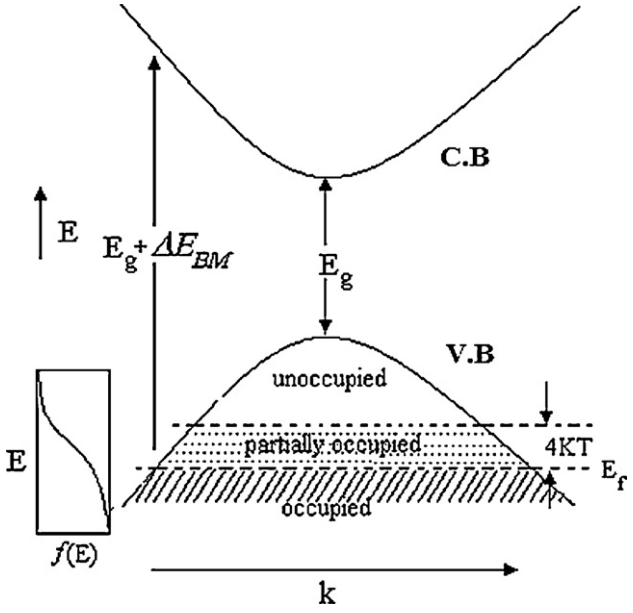

Fig. 8. Energy band diagram and optical transition across a band gap with Burstein–Moss shift.

material. Although the band gap is a characteristic property of the semiconductor and govern the optical properties, it may be shifted according to important reasons such as the energy gap confinement phenomena in nanostructured materials and the other increment of band gap by Burstein–Moss effect. In the first case, if the crystallite or particle size is comparable with the Bohr exciton radius of the $Pb_{0.9}Sn_{0.1}Se$, then the charged carriers are confined in a space which is too small to interact with each other. The contribution of such interaction is to increase the band gap by the energy of the interaction. The band gap is then calculated by the Brus formula [37,38]:

$$E_g(D) = E_{g\,bulk} + \frac{h^2}{8m_oD^2}\mu - \frac{1.8e^2}{4\pi\varepsilon_o\varepsilon_r D} - \frac{0.248 \times 4\pi^2e^4m_o}{2h^2(4\pi\varepsilon_o\varepsilon_r)\mu} \quad (3)$$

where m_o is the effective mass. $E_{g\,bulk}$ is the energy gap of bulk material. The term $(h^2m/8m_oD^2)$ is the quantum localization (*i.e.* the kinetic energy term). It obviously shifts $E_g(D)$ to higher energies. The term $(-1.8e^2/4pe_oe_rD)$ is due to the screened Coulomb interaction between the electron and the hole, it shifts $E_g(D)$ to lower energies. The last term in Eq. (3) is a size independent due to spatial correlation effects and it is usually small in both the value and the effect on $E_g(D)$ [39–43].

PbSe semiconducting material is characterized by large Bohr exciton radius of 46 nm [44,45]. At low composition, $x = 0.1$, this value does not change far from 46 nm and the energy gap confinement effect starts at crystal size close to this value while this effect decreases at higher crystallite size. The grain size measured by SEM cannot be considered due to the size of the particle surface and each particle may contained more crystallites. The X-ray diffraction measurement shows that the average crystallite sizes of the as deposited and annealed films are in the range 68–72 nm while a thin film deposited by pulsed laser technique is 40 nm. Crystallite sizes in the range 68–72 nm are considered to have minor contribution for absorption edge shift because the average crystallite size is much higher than the Bohr exciton radius of PbSnSe system. In the pulsed deposited film, the average crystallite size is close to or below the Bohr exciton radius *i.e.* The band gap or the absorption edge will be affected strongly by this critical crystallite size [46]. Although the band gap of the annealed film that deposited by evaporation is shifted below the un annealed film by 0.02 eV while there is no energy gap confinement effect in these two films. The decrease of transmittance at longer wavelength is governed only by free carriers absorption which was eliminated by annealing, *i.e.* annealing reduces the defect density and consequently reduces the free carriers concentration. According to high carriers concentration of un-annealed film and/or lower effective mass of those materials (in the range 0.1–0.3 depends on the composition), The Burstein–Moss effect plays an important role in semiconductors with high carrier concentration and/or low density of state effective mass. At low density of state effective mass materials such as Pb–Sn chalcogenide systems, increasing the charged carriers concentration moves the Fermi level towards the valance band in p-type semiconductor, (our case). Further increase in charged carriers concentration moves the Fermi level inside the valance band and the system transformed to be degenerate semiconductor in which the occupation above the Fermi level in the valance band becomes lower and the top of the valance band becomes empty. Fig. 8 explains the transition process from a point far from the zero wave vector in the energy band diagram. Transition of carrier by absorption of photon starts at a point around the Fermi level not from the top of the valance band. In this case, the photo excited carrier transit at point other than $k = 0$ in the momentum coordinate and the total difference between the lower state and higher state is observed as the energy gap with higher value than the nondegenerate case. The measured energy gap is then equal to the optical band gap of the material and twice times of the Fermi level in case that conduction band and valance band are symmetrical, In our annealed film, the resultant energy gap was about 0.12 eV due to transformation from the degenerate state to the nondegenerate state. This means that annealing process of the thermally evaporated films decreases the carriers concentration by defect removal in which the overall improvement of the film properties was happened. In the case of pulsed laser deposited films, there is no free carrier absorption due to high homogeneity of the chemical composition of the film because each laser pulse is high enough to evaporate the Pb, Sn and Se stiochiometric amount from the source by a pulse. So that defects caused by inhomogeneity are minor in this case. Fluctuation of the chemical composition in the thermal vacuum evaporation process requires annealing process at 773 K for 1 h to remove those defects.

Table 2
Photoconductivity of the pulsed laser deposited and thermal evaporated films.

	Pulsed laser deposition	Thermal vacuum evaporation
Thickness (d)	0.115 μm	0.185 μm
Width (w)	1.1 cm	1.035 cm
Length (l)	1.05 cm	1.05 cm
R_S	1.36 MΩ	2.2 kΩ
R_L	1 MΩ	2.07 kΩ
$\rho_{dark} = R_S \cdot w \times d/l$	0.164 Ω^{-1} cm^{-1}	0.4×10^{-3} Ω^{-1} cm^{-1}
$\sigma_{dark} = 1/\rho$	6.1 Ω^{-1} cm^{-1}	2500 Ω^{-1} cm^{-1}
t	18.5 ms	15.5 ms
$\Delta\sigma_{st}$ from the curve	1×10^{-7} Ω^{-1} cm^{-1}	2.5×10^{-10} Ω^{-1} cm^{-1}
Photosensitivity ($\Delta\sigma_{st}/\sigma_0$)	1.6×10^{-8}	1×10^{-13}

3.4. Photoconductive properties

The dark conductivity and resistivity were firstly measured for both films deposited by thermal evaporation and pulsed laser deposition techniques. The shape of the deposited films was controlled during the deposition process by masks. The film dimensions and corresponding resistivity are represented in Table 2. The resultant dark conductivity of the thermally evaporated film was found to be 2500 Ω^{-1} cm^{-1} while the dark conductivity of the pulsed laser deposited film was 6.1 Ω^{-1} cm^{-1}. This result is compatible with the free carriers that found in the thermally evaporated films which contribute directly to the overall carriers concentration. Conductivity contains two main components; they are the mobility and carriers concentration for each type of conduction. It was believed that mobilities of the two films are close to each other because of the polycrystalline structure, small grain size and the same overall composition and they were deposited on the same substrate. So that the difference between them is considerably low. The frequency dependence of photoconductivity is hyperbolic function of the frequency and lifetime and follows the equation [47]:

$$\Delta\sigma = \Delta\sigma_{st} \tanh\left(\frac{1}{4\tau f}\right) \quad (4)$$

where $\Delta\sigma$ and $\Delta\sigma_{st}$ are photoconductivity and its steady state value (at very low chopping frequency). It is normally determined by extrapolation of low frequency dependence photoconductivity. Normalization of the photoconductivity and plotting it with the chopping frequency results a hyperbolic curve as shown in Fig. 9. According to Eq. (4), at the point of $tanh(1)$ equal 0.76 of the normalized photoconductivity axis, one can determine the carrier lifetime which equal $1/(4f)$. The carriers lifetime in the both films are in the same order of magnitude and equal 18.5 and 15.5 ms for films deposited by pulsed laser deposition and thermal vacuum evaporation, respectively. It is also observed that those lifetimes are lower than the characteristic carrier lifetime of the single crystal about several μs [15]. this means that our

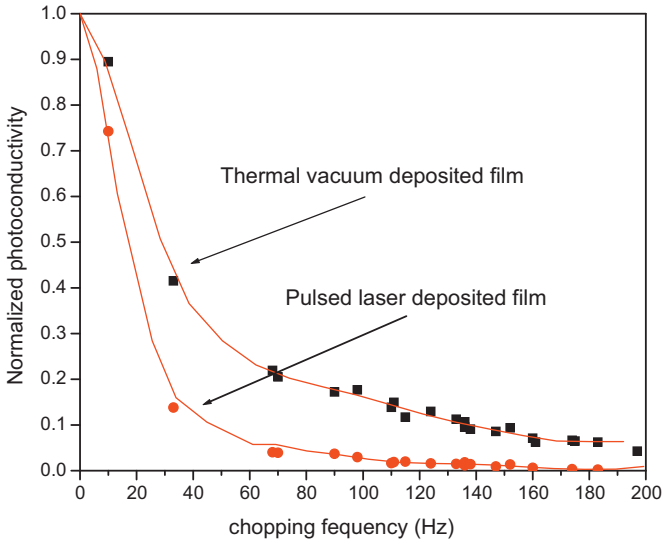

Fig. 9. Chopping frequency dependence of photoconductivity for $Pb_{0.9}Sn_{0.1}Se$ films.

measurements of frequency dependence of photoconductivity in the frequency range 0–200 Hz are limited to measure only the long-range lifetime. Long-range carrier lifetime is the characteristic generation-recombination duration time across the grains. It occurs only as a resultant of scattering process by grain boundaries scattering. There are many scattering processes and corresponding carrier lifetimes while the only observed at this frequency range and room temperature is the long-term carrier lifetime. The characteristic carrier lifetime of single crystallite can be observed at much higher chopping frequency which is out of our experimentation measurement conditions. There are several reports on the IV–VI materials such as $Pb_{1-x}Sn_xTe$ with different compositions. They were deposited by thermal, flash and electron beam evaporation techniques that their carriers mobilities was much smaller than single crystal while their long-term carrier lifetime dominates the photoconduction process at room temperature and lower chopping frequency [33–35]. It can be concluded that thin poly and nanocrystalline film deposited by the mentioned technique possess photoconduction relaxation curves that are controlled by long-term carrier lifetime. Then the photocarriers are mainly generated and recombined at the interfaces between grains higher than generation and recombination inside the grain itself. The difference in carrier lifetimes of both films deposited by thermal and PLD evaporation shows a difference in the long-term carrier lifetime itself. Besides this observation was noticed in the rise–decay relaxation curves. The dynamic of the rise and decay curves were taken by fast digital camera at the same chopping frequency from the oscilloscope and represented in pictures of Fig. 10. It was observed

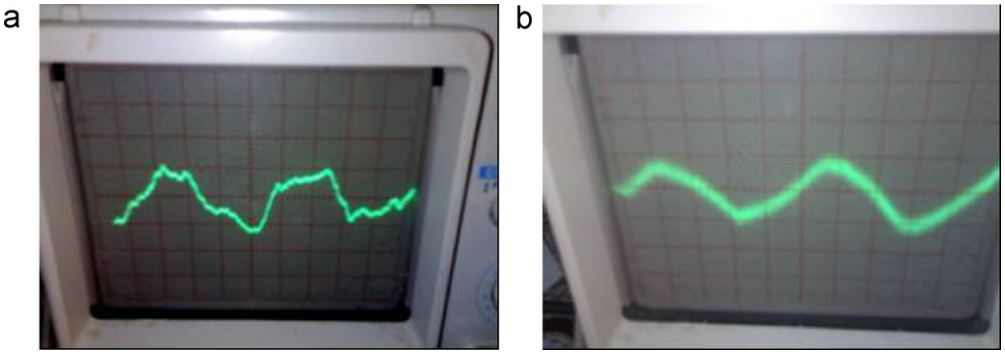

Fig. 10. Photoconductivity relaxation curve (a) thermal evaporated film (b) pulsed laser deposited film.

that, the pulsed laser deposited film has minor noise (high signal to noise ratio) while in the thermally deposited film the noise is seen clearly at the relaxation curve. Besides, the rise and decay curves are slower than those for thermally deposited film. Table 2 summarizes the photoconductivity parameters and results. The most important result is that the photosensitivity which the photoconductivity divided by the dark conductivity which governs the photoconductor performance and signal to noise ratio in photo detectors device application. Thin films or photoconductor deposited by thermal vacuum deposition has photosensitivity smaller than the photoconductor deposited by pulsed laser technique by five orders of magnitude. This indicates the high photosensitivity and strong performance of such IR photoconductor deposited by thermal deposition technique for signal detecting process. This difference is attractive for high photosensitivity thermal imaging applications. It is also important to mention that photoconductors deposited by thermal evaporation technique has carriers lifetime shorter than that of film deposited by pulsed laser technique. This result is also attractive for high speed optoelectronics with lower photosensitivity in compared with photoconductors deposited by pulsed laser technique.

4. Conclusions

From the above comparative study it can be concluded that:

1. Thermal vacuum evaporation and pulsed laser deposition techniques produce $Pb_{0.9}Sn_{0.1}Se$ thin films with good quality and considrable high performance with some difference in their optoelectronic proerties.
2. Energy gap of thermally deposited films increased due to Burstein–Moss effect and free carriers were also abserved and both of them were reduced by annealing at 773 K for 1 h.
3. Energy gap of pulsed laser deposited film was highly increased due to confinment effect of band gap in nanosized $Pb_{0.9}Sn_{0.1}Se$ thin films.
4. Thermally deposited films possesses faster optoelectronic process than the pulsed laser deposited film while the later are more photosensitive one.

Acknowledgments

This work was carried out through the support of the City for Scientific Research and Technology Applications and collaboration research with the National Institute of Laser Enhanced Science.

References

[1] A.M. Samoylov, M.K. Sharov, S.A. Buchnev, A.M. Khoviev, E.A. Dolgopolova, J. Cryst. Growth 240 (2002) 340.
[2] M.S. Dresselhaus, G. Dresselhaus, X. Sun, Z. Zhang, S. Cronin, T. Koda, J.Y. Ying, Microsc. Therm. Eng. 3 (1999) 89.
[3] H. Zogg, M. Arnold, Infrared Phys. Technol. 49 (2007) 183.
[4] I.N. Chao, P.J. McCann, W.L. Yuan, E.A. Orear, S. Yuan, Thin Solid Films 323 (1998) 126.
[5] M. Hennie, Narrow Band Gap, III–VI, vol. 7, 1994, p. 44.
[6] H. Zogg, Thin Film Physics Group (Gruppe Dünnschichtphysik) Annual Report, 1999, p. 4.
[7] Long and Schmit 1973; Dingyuan Tang, 1976.
[8] K.H. Herrmann, V. Melzer, Infrared Phys. Technol. 37 (1996) 753.
[9] M. Tacke, A. Ishida, Optical Properties IV–VI Semiconductors Part 1, vol. 34C1, 2001.
[10] R.J. Cushman, Proc. IRE 47 (1959) 1471.
[11] H. Preier, J. Appl. Phys. 10 (1979) 189.
[12] F.J. Meca, M.M. Quintas, F.J.R. Sanchez, Sens. Actuators 84 (2000) 45.
[13] Z. Dashevsky, S. Shusterman, M.P. Dariel, J. Appl. Phys. 92 (2002) 1425.
[14] D. Khokhlov (Ed.), Lead Chalcogenides: Physics and Applications, Taylor & Francis, New York, 2003, p. 76.
[15] V.V. Tetyorkin, A.Yu. Sipatove, F.F. Sizov, A.I. Fedorenko, A. Fedrov, Infrared Phys. Technol. 37 (1996) 379.
[16] B. Li, Y. Xie, Y. Xu, C. Wu, Z. Li, J. Solid State Chem. 179 (2006) 56.
[17] I.C. Baek a, S.I. Seok, N.C. Pramanik, S. Jana, M.A. Lim, B.Y. Ahn, C.J. Lee, Y.J. Jeong, J. Colloid Interface Sci. 310 (2007) 163.
[18] B.R. Sankapal, R.D. Ladhe, D.B. Salunkhe, P.K. Baviskar, V. Gupta, S. Chan, J. Alloy Compd. 509 (2011) 10066.
[19] A. Osherov, M. Shandalov, V. Ezersky, Y. Golan, J. Cryst. Growth 304 (2007) 169.
[20] P.K. Khanna, N. Singh, S. Charan, A.K. Viswanath, K.R. Patil, Mater. Res. Bull. 42 (2007) 1414.
[21] M. Shandalova, Z. Dashevsky, Y. Golan, Mater. Chem. Phys. 112 (2008) 132.
[22] T.N. Xu, H.Z. Wu, J.X. Si, C.F. Cao, Appl. Surf. Sci. 253 (2007) 5457.
[23] K.K. Zhuravlev, Physica B 394 (2007) 1.
[24] D. Li, J. Maa, S. Mukherjee, G. Bi, F. Zhao, S.L. Elizondo, Z. Shi, J. Cryst. Growth 311 (2009) 3395.
[25] M. Suzuki, T. Seki, Thin Solid Films 343–344 (1999) 317.
[26] D.K. Ivanou, E.A. StreltsovT, A.K. Fedotov, A.V. Mazanik, Thin Solid Films 487 (2005) 49.
[27] P. Bajaj, E. Woodruff, J.T. Moore, Mater. Chem. Phys. 123 (2010) 581.
[28] E.A.A. El-Shazly, I.T. Zedan, K.F. Abd El-Rahman, Vacuum 86 (2011) 318.
[29] V. Arivazhagan, M. Manonmani Parvathi, S. Rajesh, doi:10.1016/j.vacuum.2011.10.008.
[30] D.W. Ma, C. Cheng, J. Alloy Compd. 509 (2011) 6595.
[31] W. Lv, X. Wang, Q. Qiu, F. Wang, Z. Luo, W. Weng, J. Alloy Compd. 493 (2010) 358.
[32] U. Kumara, S.N. Sharma, S. Singh, M. Kara, V.N. Singh, B.R. Mehta, R. Kakkard, Mater. Chem. Phys. 113 (2009) 107.
[33] F.S. Terra, M. Abdel Rafea, M. Monir, J. Mater. Sci. Mater. Electron. 12 (2001) 561.
[34] M. Abdel Rafea, F.S. Terra, M. Mounir, R. Labusch, Chalcogenide Lett. 6 (3) (2009) 115.
[35] M. Abdel Rafea, R. Labusch, F.S. Terra, M. Mounir, J. Optoelectron. Adv. Mater. RC 3 (2009) 543.
[36] R.V. Stuart, Vacuum Technology, Thin Films and Sputtering, Academic Press, London, 1983, p. 65 (Chapter 3).
[37] Y. Shani, R. Rosman, Katzir, J. Quantum Electron. 21 (1985) 51.
[38] H. Demiryont, J.R. Sites, K. Geib, J. Appl. Opt. 24 (1985) 490.
[39] P.R. Yoder, Opto-Mechanical Systems Design, third ed., CRC Press, 2006.
[40] A. Vomvasi, K. Pomonti, C. Traplis, N. Todorova, Mater. Sci. Poland 25 (2007) 3.
[41] Hand Book of Solid State Lasers/edited by Peter K. Cheo.P.cm. (optical engineering; v.18), ISBN 0-8247-7857-X.
[42] C. Suryanarayana, Mechanical Alloying and Milling, ISBN 0-8247-4103-x.
[43] M.J. Buergers, Crystal Structure Analysis, Wiley, New York/London, 1960.
[44] L.E. Brus, J. Chem. Phys. 79 (1983) 5566.
[45] L.E. Brus, J. Chem. Phys. 80 (1984) 4403.
[46] B. Pejova, I. Grozdanov, Mater. Lett. 58 (2004) 666.
[47] S.M. Ryvkin, Photoelectric Phenomenon in Semiconductors, New York, 1964 (Chapter 3).